JOURNAL OF SPACECRAFT AND ROCKETS
Vol. 46, No. 3, May–June 2009

Influence of Ablation on Radiative Heating for Earth Entry

Christopher O. Johnston* and Peter A. Gnoffo†
NASA Langley Research Center, Hampton, Virginia 23681
and
Kenneth Sutton‡
National Institute of Aerospace, Hampton, Virginia 24060

DOI: 10.2514/1.40290

Using the coupled ablation and radiation capability recently included in the LAURA flowfield solver, this paper investigates the influence of ablation on the shock-layer radiative heating for Earth entry. The extension of the HARA radiation model, which provides the radiation predictions in LAURA, to treat a gas consisting of the elements carbon, hydrogen, oxygen, and nitrogen is discussed. It is shown that the absorption coefficient of air is increased with the introduction of the carbon and hydrogen elements. A simplified shock-layer model is studied to show the impact of temperature, as well as the abundance of carbon and hydrogen, on the net absorption or emission from an ablation contaminated boundary layer. It is found that the ablation species reduce the radiative flux in the vacuum ultraviolet, through increased absorption, for all temperatures. However, in the infrared region of the spectrum, the ablation species increase the radiative flux, through strong emission, for temperatures above 3000 K. Thus, depending on the temperature and abundance of ablation species, the contaminated boundary layer may either provide a net increase or decrease in the radiative flux reaching the wall. To assess the validity of the coupled ablation and radiation LAURA analysis, a previously analyzed Mars-return case (15.24 km/s), which contains significant ablation and radiation coupling, is studied. Exceptional agreement with previous viscous-shock-layer results is obtained. A 40% decrease in the radiative flux is predicted for ablation rates equal to 20% of the freestream mass flux. The Apollo 4 peak-heating case (10.24 km/s) is also studied. For ablation rates up to 3.4% of the freestream mass flux, the radiative heating is reduced by up to 19%, whereas the convective heating is reduced by up to 87%. Good agreement with the Apollo 4 radiometer data is obtained by considering absorption in the radiometer cavity. For both the Mars-return and the Apollo 4 cases, coupled radiation alone is found to reduce the radiative heating by 30–60% and the convective heating by less than 5%.

Nomenclature

$\tilde{c}_i$	=	elemental mass fraction of element i
hv	=	frequency in electron volts
$m\text{-}dot$	=	ablation or mass injection rate divided by the freestream density and velocity
q_c	=	convective heating, W/cm^2
q–cumulative	=	running total of the spectrally integrated radiative heat flux, starting at 0 eV, W/cm^2
q_r^-	=	wall-directed radiative flux, W/cm^2
T_i	=	temperatures for the simplified shock-layer model, $i = 1$ and 2 for layers 1 and 2
T_{tr}	=	translational-rotational temperature
T_{ve}	=	vibrational-electronic-electron temperature
x	=	coordinate parallel to the freestream or along the stagnation line, cm
z	=	coordinate normal to freestream, m
α	=	mass fraction of ablation species in air/ablation mixture
Δz_i	=	thickness of the constant-property layers defined with $i = 1$ or 2, cm
κ_{h_v}	=	absorption coefficient, cm^{-1}
λ	=	blowing reduction parameter
Φ	=	transmissivity

Subscript

hv	=	indicates a spectral dependence in terms of electron volts

Superscripts

abl	=	refers to ablation species, meaning species containing any carbon or hydrogen atoms
air	=	refers to air species, meaning species containing no carbon or hydrogen atoms

Presented as Paper 4107 at the 40th AIAA Thermophysics Conference, Seattle, WA, 23–26 June 2008; received 6 August 2008; accepted for publication 2 April 2009.

*Aerospace Engineer. Member AIAA.
†Aerospace Engineer. Fellow AIAA.
‡Senior Research Fellow. Associate Fellow AIAA.

I. Introduction

THE design of the ablating heat shield for NASA's Orion crew module requires the accurate prediction of the shock-layer radiative and convective heating. The ablating heat shield introduces carbon and hydrogen species into the flowfield, which complicate the flowfield and radiation modeling. The influence of these ablation products at peak-heating lunar-return conditions, approximately defined by a velocity of 10.5 km/s, an altitude of 70 km, and a non-dimensional ablation rate ranging from 0.005 to 0.05, is of particular interest for Orion. The nondimensional ablation rate $m\text{-}dot$ is defined as the ablation rate divided by the freestream velocity and density (or freestream mass flux).

Previous studies concerning the influence of ablation on the radiative heating have reported both increases and decreases in the radiative heating with the introduction of ablation. Research in the late 1960s [1–3] and early 1970s [4–9], which was based mostly on equilibrium viscous-shock-layer flowfield models and 1960s-era radiation data, showed a radiation decrease of roughly 30% with $m\text{-}dot$ values of 0.05 for conditions relevant to Mars return (15.24 km/s at 60.96 km). A later analysis by Gupta et al. [10] confirmed these results with an updated flowfield model. More recent studies have focused on the analysis of the Apollo 4 flight data [11] and the design and analysis of the Stardust [12–14] and MUSES-C

[15] vehicles. For the Stardust [12] and Apollo [11] cases, Park predicts a significant reduction in the wall radiative flux due to vacuum ultraviolet absorption from ablation products, with *m-dot* ranging from 0.0086 to 0.03. In contrast to the large radiation decrease shown by Park [11,12], both Olynick et al. [13] and Gupta [14] predict a slight *increase* in the radiative heating due to ablation species for Stardust peak-heating conditions. For entry of the MUSES-C vehicle [16], which is similar to the Stardust vehicle, both Doihara and Nishida [15] and Otsu et al. [17] predict a 20% increase in the radiation with the introduction of ablation, whereas Fujita et al. [18] predict a negligible change.

The influence of ablation on the radiative heating has been examined for entry into atmospheres other than Earth. Analyses by Nicolet [19], Moss et al. [20,21], and Arnold et al. [22] in the late 1970s considered the entry of the Galileo probe into Jupiter. These studies showed that the radiative heating, resulting mostly from hydrogen, was reduced by up to 50% with the introduction of ablation. The *m-dot* values for these cases ranged from 0.05 to 0.5, whereas the shock-layer temperatures were on the order of 15,000 K. The presence of a turbulent boundary layer was shown by Moss et al. [23] and Matsuyama et al. [24] to have a significant impact on the radiative heating for the Galileo probe. It was shown that turbulence increased the temperatures near the wall and altered the species diffusion, therefore reducing the number of absorbing molecules (such as C_3) in the boundary layer. For the Venus entry of the Pioneer Venus probes, a reduction in the radiative heating due to ablation products of roughly 20% was predicted by Moss et al. [25], whereas Park and Ahn [26] predicted a reduction of about 50%. The *m-dot* values for these cases were below 0.02. Studies of entry into Venus by Sutton [27] and Fujita et al. [28–30] have shown about a 20% reduction in the radiative heating by ablation. For Mars entry, with an *m-dot* of 0.075, Gupta et al. [31] predicted a radiative heating reduction of 50% with the introduction of ablation.

The conflicting trends found by previous studies, as noted in the preceding paragraphs, for the influence of ablation on radiative heating motivated the present study. Applying state-of-the-art flowfield (LAURA) and radiation (HARA) models, the present work examines the influence of ablation on the radiative heating for lunar- and Mars-return conditions. A brief discussion of this recently developed capability [32], which consists of a 22-species thermochemical nonequilibrium LAURA flowfield model with coupled HARA radiation and an ablating wall, is discussed in Sec. II. In Sec. III, the extension of HARA to treat carbon and hydrogen species is discussed and the sources of the required data are listed. The influence of the additional carbon and hydrogen species on the emission and absorption in an ablating boundary layer are examined in Sec. IV, using a simplified shock-layer model consisting of two constant-property layers, which allows the influence of the ablation species to be easily observed and interpreted. In Sec. V, the coupled ablation and radiation solutions for a widely studied Mars-return case is presented to provide confidence in the present analysis. The influence of the ablation and radiation coupling on the radiative and convective heating for the Apollo 4 peak-heating case are examined in Sec. VI, and a comparison is made with the flight data.

II. Flowfield Modeling with Ablation Products and Radiation

The Langley Aerothermodynamic Upwind Relaxation Algorithm (LAURA) is a high fidelity, structured grid analysis tool, specialized for hypersonic reentry physics, using state-of-the-art algorithms for computational fluid dynamic simulations [33,34]. Key elements of LAURA include Roe's averaging [35] and Yee's symmetric total variation diminishing (STVD) [36] formulation of second-order, inviscid flux. Yee's STVD formulation has been found to be exceptionally robust and Courant-number-independent using first point-implicit and then line-implicit relaxation for hypersonic flow simulations.

A two-temperature thermochemical nonequilibrium model [34] is applied, except in Sec. V, in which a single temperature chemical equilibrium model is applied. The following 22 species are included in the flowfield calculation: N, N^+, NO, NO^+, N_2, N_2^+, O, O^+, O_2, O_2^+, C, C^+, CO, CO_2, C_2, C_3, C_2H, CN, H, H^+, H_2, and e^-. The chemical reaction rates are compiled from previous studies of Earth [37,38], Mars [39], and Titan [40] entry. The thermophysical properties are taken from the work of Mcbride et al. [41] and Gupta et al. [42]. Multicomponent diffusion is approximated using Sutton and Gnoffo's [43] approximate-corrected approach. Values of 0.76 and 0.24 are applied for the freestream elemental mass fractions of nitrogen and oxygen, respectively.

Laminar flow is assumed for all cases. As mentioned in the Introduction, past studies [23] of the strongly ablating and radiating Galileo probe showed an influence of turbulent flow on the radiation. Preliminary results were obtained for the Apollo 4 case presented in Sec. VI using the standard Baldwin–Lomax algebraic turbulence model. For the *m-dot* values considered, these results showed a negligible influence of turbulence on the radiative heating, although the convective heating was significantly increased. No attempt was made to alter the applied turbulence model to account for ablation. The proper treatment of turbulence in the presence of ablation was beyond the scope of the present work, although it should be considered in a future study.

The treatment of a blowing boundary condition in LAURA was presented by Thompson and Gnoffo [44]. Recent work [32] has extended this capability to accommodate the injection of a gas containing the elements C, H, O, and N. The wall is assumed to be in chemical equilibrium at a specified wall temperature. The elemental composition at the wall is obtained by solving the elemental continuity equations [45], which account for diffusion, convection, and mass injection of the char and pyrolysis gas. For cases with no ablation, these equations reduce to the equilibrium catalytic wall conditions. The ablation rate and elemental composition of the injected char and pyrolysis gas are specified along with the wall temperature. Although the ablation rate at the stagnation point is specified, the distribution along the rest of the body is scaled with the local wall pressure.

The divergence of the radiative flux, calculated from the HARA code, is included in the LAURA flowfield calculations. For typical lunar-return cases, the radiation is updated every 3000 flowfield iterations. Details of the HARA code are provided in the following section.

III. Radiation Modeling of Air with Ablation Products

The shock-layer radiation is modeled with the HARA (high-temperature aerothermodynamic radiation) code. The details of this code for treating air species are presented by Johnston et al. [46,47]. Briefly, it is based on a set of atomic levels and lines obtained from the National Institute of Standards and Technology (NIST) online database [48] and the Opacity Project [49], as well as atomic bound-free cross sections from the TOPbase [50]. The negative nitrogen and oxygen ions are treated using cross sections suggested by Soon and Kunc [51] and Chauveau et al. [52], respectively. The molecular band systems are treated using a smeared-rotational band (SRB) model [53], which was shown by Johnston et al. [46] to be sufficient for treating vacuum ultraviolet (VUV) absorbing and optically thin emitting band systems in air. The accuracy of the SRB model for treating band systems resulting from ablation species is discussed in Sec. IV. The molecular data for modeling these band systems are obtained from Laux [54], except for the VUV N_2 systems, which are obtained from various other sources [55–57]. The non-Boltzmann modeling of the atomic and molecular electronic states is based on a set of electron-impact excitation rates compiled from the literature and presented in detail by Johnston et al. [47]. Following the work of Park [58], the quasi-steady-state assumption is made when solving the master equation. The tangent-slab approximation is applied to calculate radiative flux and the divergence of the radiative flux, which is required for the radiation-flowfield coupling procedure. For calculating the divergence of the radiative flux, the wall is assumed to emit with an emissivity of 0.85 at the specified wall temperature. Note that the radiative flux emitted from the wall is not included in the wall radiative heating values presented throughout this paper.

This is clarified by referring to the presented values as the "wall-directed radiative flux at the wall," represented as q_r^-.

For the present study, the HARA code was extended to treat hydrogen and carbon ablation species. The various radiative mechanisms for these species are listed in Table 1. For atomic carbon and hydrogen, the oscillator strengths and electronic levels from NIST are applied. In addition, the Stark broadening widths from Griem [59] and Wilson and Nicolet [60] are used for carbon, whereas, for hydrogen, the line shapes and broadening parameters presented by Sutton [61] are applied. The photoionization cross sections for carbon and hydrogen are obtained by curve fitting the detailed TOPbase [50] cross sections. For the molecular band oscillator strengths and energy level data, the values presented by Lino da Silvia and Dudeck [62] are applied for many of the C_2 and CO systems, except for the CO VUV systems, which were obtained from Park [63]. For the CN and H_2 systems, values from Laux [54] and Allison and Dalgarno [67] are applied. For the C_3 and C_2H band systems, the available data [64–66] is limited to experimentally determined total cross sections, which are essentially constant with temperature.

Radiation emission and absorption from spalled particles [68,69] are not treated in this study, although Park has predicted that the emission from these particles contributes significantly to the radiative heating for the Stardust vehicle [12]. Note that there is significant uncertainty in the modeling parameters required to treat this mechanism. Also, postflight analyses of the Stardust heat shield recession [70] and observed radiation [71] data do not indicate the presence of excessive radiation that may be attributed to spalled particle emission. The same is true for the present analysis of the Apollo 4 flight data presented in Sec. VI, where good agreement with the flight data is found without accounting for spalled particle emission. This argument does not rule out spalled particle *absorption*, or blockage, which may reduce the radiative flux reaching the wall. However, the magnitude of this absorption mechanism is likely small [69].

For the air and ablation species mixtures to be studied in Sec. IV for the simplified shock-layer model, the parameter α is defined to represent the mass fraction of ablation elements in an air/ablation mixture. The elemental mass fractions of the mixture are then defined as

Table 1 Radiative mechanisms treated for ablation species

Species	Mechanism	Spectral range, eV	Reference
C	Lines	0–18	[48,59,60]
	Photoionization	0–18	[50]
H	Lines	0–18	[48,61]
	Photoionization	0–18	[50]
CO	$4+(A^1\Pi - X^1\Sigma)$	6.0–10	[62]
	$3+(b^3\Sigma - a^3\Pi)$	3.0–5.0	[62]
	$B^1\Sigma - X^1\Sigma$	10.2–11.4	[63]
	$C^1\Sigma - X^1\Sigma$	10.0–12.2	[63]
	$E^1\Pi - X^1\Sigma$	11.2–11.9	[63]
	Angstrom $(B^1\Sigma - A^1\Pi)$	0.5–3.2	[62]
	Asundi $(a^3\Sigma - a^3\Pi)$	0.1–3.5	[62]
	Triplet $(d^3\Delta - a^3\Pi)$	0.1–4.0	[62]
C2	Swan $(d^3\Pi - a^3\Pi)$	0.4–4.2	[62]
	Phillips $(A^1\Pi - X^1\Sigma)$	0.1–2.7	[62]
	Balik–Ramsay $(b^3\Sigma - a^3\Pi)$	0.1–2.2	[62]
	Deslandres–d'Azambuja $(C^1\Pi - A^1\Pi)$	1.5–4.5	[62]
	Mulliken $(D^1\Sigma - X^1\Sigma)$	3.6–7.4	[62]
	Fox–Herzberg $(e^3\Pi - a^3\Pi)$	3.0–6.2	[62]
C_3	Swings $(A^1\Pi - X^1\Sigma)$	2.5–4.1	[64]
	$UV^1\Sigma - X^1\Sigma$	7.3–10	[65]
C_2H	Continuum	4.6–6.5	[66]
CN	Violet $(B^1\Sigma - X^1\Sigma)$	2.6–4.0	[54]
	Red $(A^1\Pi - X^1\Sigma)$	0.5–1.5	[54]
H_2	Lyman $(B^1\Sigma - X^1\Sigma)$	10–14.0	[67]
	Werner $(C^1\Pi - X^1\Sigma)$	8.1–12.3	[67]

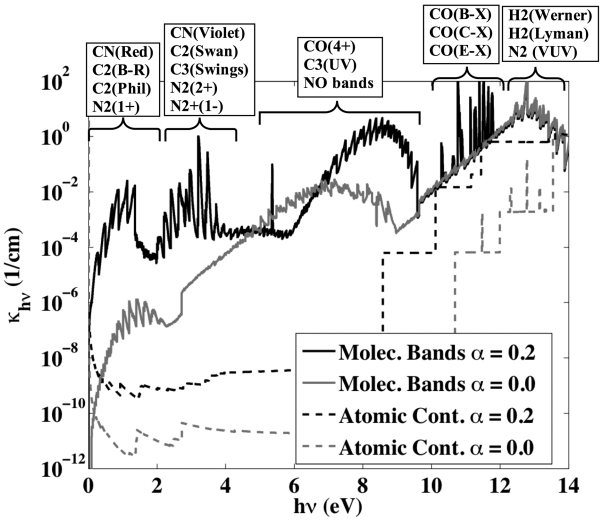

Fig. 1 Absorption coefficients at 5000 K and 0.5 atm resulting from molecular band systems and atomic photoionization for pure air ($\alpha = 0.0$) and a mixture of ablation gas and air ($\alpha = 0.2$).

$$\tilde{c}_i = \tilde{c}_i^{\text{air}}(1-\alpha) + \tilde{c}_i^{\text{abl}}\alpha \quad \tilde{c}_{\text{N}}^{\text{air}} = 0.76, \quad \tilde{c}_{\text{O}}^{\text{air}} = 0.24, \quad \tilde{c}_{\text{C}}^{\text{air}} = 0.00$$
$$\tilde{c}_{\text{H}}^{\text{air}} = 0.0 \quad \tilde{c}_{\text{N}}^{\text{abl}} = 0.04, \quad \tilde{c}_{\text{O}}^{\text{abl}} = 0.01, \quad \tilde{c}_{\text{C}}^{\text{abl}} = 0.90, \quad \tilde{c}_{\text{H}}^{\text{abl}} = 0.05 \tag{1}$$

Therefore, $\alpha = 0.0$ represents pure air, whereas a value greater than zero represents a mixture of air and ablation species. Figure 1 presents the total molecular band and atomic continuum absorption coefficients for pure air ($\alpha = 0.0$) and for a mixture of air and ablation species ($\alpha = 0.2$). It is seen that, for the same temperature and pressure, both the molecular band and atomic continuum absorption coefficients are significantly larger over most of the spectrum. The $\alpha = 0.0$ molecular band result is larger in the region between 4 and 6 eV because of the strong NO band systems. For the $\alpha = 0.2$ case, most of the NO is replaced by CO, which increases the spectrum in the 7–9 eV range, but decreases it in the 4–6 eV range. Figure 2 shows the impact of this increased absorption on a 1-cm constant-property layer. The transmissivity Φ, which represents the fraction of the intensity that passes through the layer, is defined as

$$\Phi = \exp(-\kappa_{h\nu}\Delta z) \tag{2}$$

where $\kappa_{h\nu}$ is the absorption coefficient and Δz is the thickness of the layer. For clarity, the atomic line contribution is not included in the figure. Therefore, the sum of the band and continuum absorption coefficients shown in Fig. 1 are applied for this example. Above 12 eV, it is seen that Φ is essentially zero for both cases, which means that all of the radiation entering the layer in this spectral range is absorbed. The most significant difference between the two cases is in the 6–10 eV range, where the $\alpha = 0.2$ case contains significantly more absorption. This is a result of the CO (4+) and C_3 (UV) band systems. The impact of these transmissivity differences on the radiative flux or intensity passing through the layer depends on the spectral distribution of the incoming flux or intensity. For typical lunar-return shock-layer conditions, this impact will be shown in the next section. The increase in the absorption coefficient shown here indicates a corresponding increase in the emission coefficient. The net effect of the increased emission and absorption for a simplified ablating boundary layer will also be studied in the next section.

IV. Radiation Analysis of a Simplified Ablating Shock Layer

For insight into the absorption and emission of an ablating shock layer, a simplified model will be examined [72,73]. This model, shown in Fig. 3, consists of a high-temperature layer of air (layer 1), and a smaller, lower-temperature layer containing both air and ablation species (layer 2). To approximate the inviscid region of a

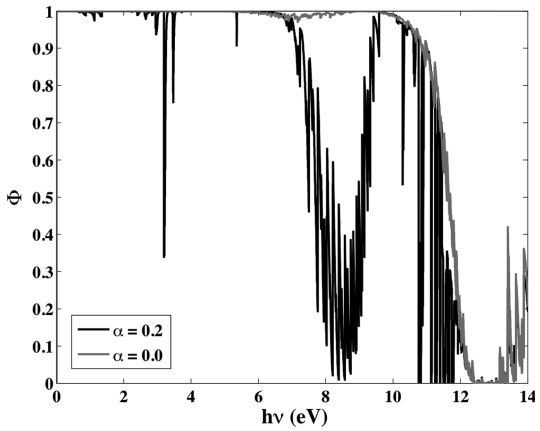

Fig. 2 Transmittance through a 1-cm layer at 5000 K and 0.5 atm resulting from pure air ($\alpha = 0.0$) and a mixture of ablation gas and air ($\alpha = 0.2$).

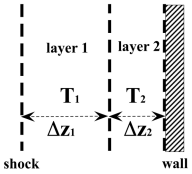

Fig. 3 Simplified shock-layer model.

lunar-return shock layer, T_1 and Δz_1 are set to 10,000 K and 15 cm, respectively. To approximate the boundary layer, T_2 will be varied, whereas Δz_2 is set to 1 cm. The pressure in both layers is set to 0.5 atm.

For various values of T_2 and α, the spectrally integrated radiative flux to the wall of the simplified shock-layer model is presented in Figs. 4a–4c. Figure 4a shows that, for T_2 values greater than 3000 K, layer 2 provides a net increase in the flux below 6 eV, meaning the emission in these cases is larger than the absorption. For the flux above 6 eV, Fig. 4b shows that, for all values of T_2 and α, layer 2 absorbs a significant fraction of the flux from layer 1. The amount of absorption is seen to increase with increasing α. Figure 4c presents the entire flux, which is the sum of the values in Figs. 4a and 4b. A slight minimum is apparent at $\alpha = 0.1$ for temperatures above 3000 K. The 3000 K case is the only case with a continuous decrease in the flux with increasing α. Note that the largest flux for $\alpha > 0.2$ is from the 5000 K case, and not the 6000 K case. For all cases with $\alpha < 0.3$, layer 2 provides net absorption, meaning the flux from layer 2 is less than that from layer 1.

To further investigate these trends, Figs. 5a–5c present the cumulative flux spectrums from layer 2 for several of the cases presented in Figs. 4a–4c. The increase in the emission between 1–3 eV as α is increased may be attributed to the C_2, C_3, and CN bands identified in Fig. 1. The flux above 12 eV is seen to be absorbed for all cases, which is consistent with the nearly zero transmittance shown in Fig. 2 for this spectral range (even for the $\alpha = 0$ case). The introduction of ablation species were shown in that figure to reduce the transmittance considerably between 7 and 9 eV. As a result, Figs. 5b and 5c show a reduced flux contribution from this spectral range relative to the pure air case in Fig. 5a.

As mentioned in the previous section, the HARA code applies the smeared-rotational band model for treating the molecular band systems. Although this model is known to be accurate for optically thin emission [74], its ability to treat optically thick absorption is questionable. The significant absorption from VUV molecular band systems shown in Figs. 1 and 2 indicates that significant optically thick absorption is encountered in an ablating or non-ablating boundary layer. The sufficient accuracy of the SRB model for the VUV absorption in a nonablating boundary layer was shown by Johnston et al. [46]. To assess the validity of the SRB model in the presence of ablation species, Fig. 6a presents the VUV flux

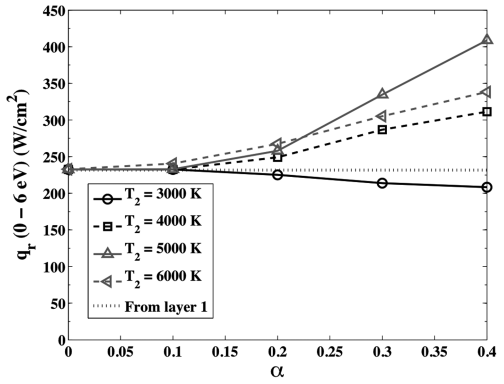

a) Radiative flux between 0 and 6 eV

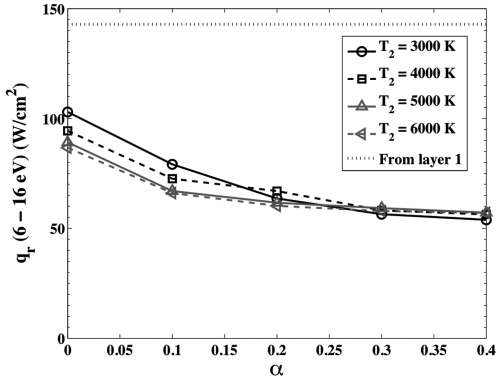

b) Radiative flux between 6 and 18 eV

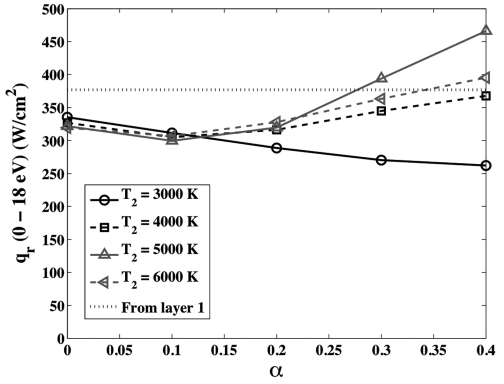

c) Radiative flux between 0 and 18 eV

Fig. 4 Radiative flux toward the wall of the simplified shock-layer model shown in Fig. 3.

spectrum from layer 2 for $\alpha = 0.4$ and $T_2 = 5000$ K. The corresponding cumulative flux above 8 eV is presented in Fig. 6b. In both of these figures, the fluxes obtained by ignoring all VUV-band systems are represented by dashed lines. Likewise, the flux obtained by treating all VUV-band systems with a line-by-line (LBL) or SRB model are represented by the solid gray and black lines, respectively. The LBL curve in Fig. 6a appears as a solid area because of the numerous closely spaced rotational lines. The absorption from the VUV-band systems is indicated by the difference between the LBL or SRB results and the no VUV-bands case. It is seen from Fig. 6b that over 40% of the VUV flux is absorbed by the VUV-band systems. Furthermore, it is seen that the cumulative VUV fluxes predicted by the LBL and SRB models agree within 3%, even though there are noticeable differences in the spectrums shown in Fig. 6a. Further discussion on the validity of the SRB model in the VUV is found in [46]. Similar results were observed for other α and

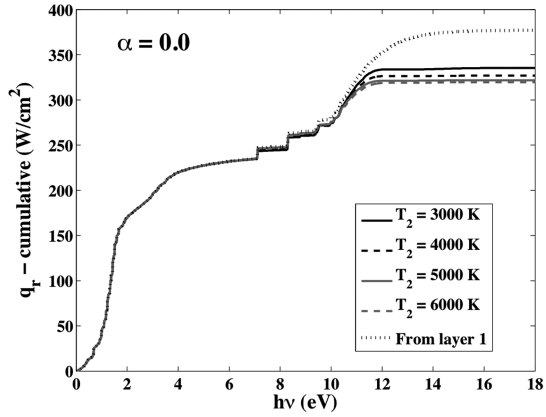

a) $\alpha = 0.0$ (air)

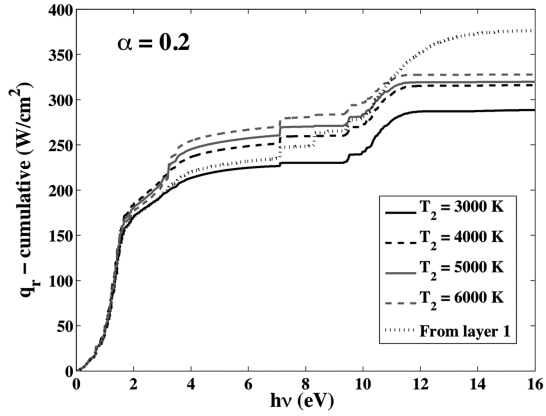

b) $\alpha = 0.2$

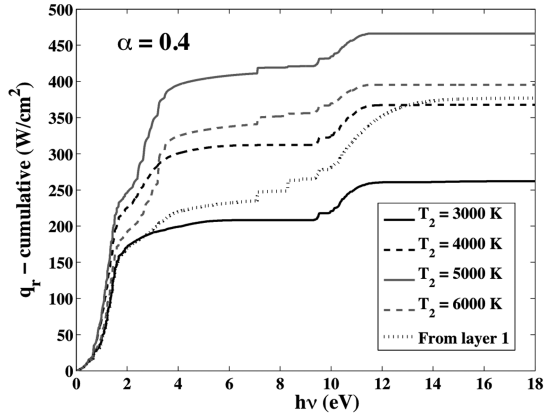

c) $\alpha = 0.4$

Fig. 5 Cumulative flux toward the wall of the simplified shock-layer model shown in Fig. 3.

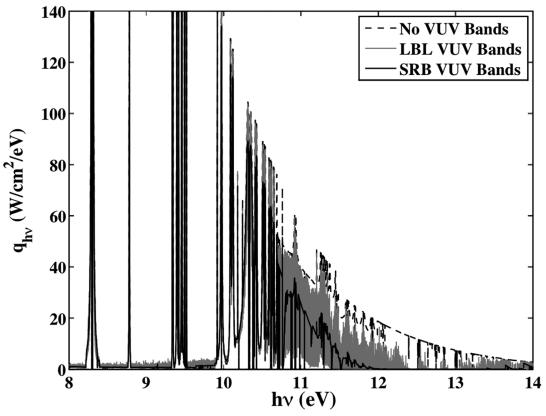

a) Spectral flux

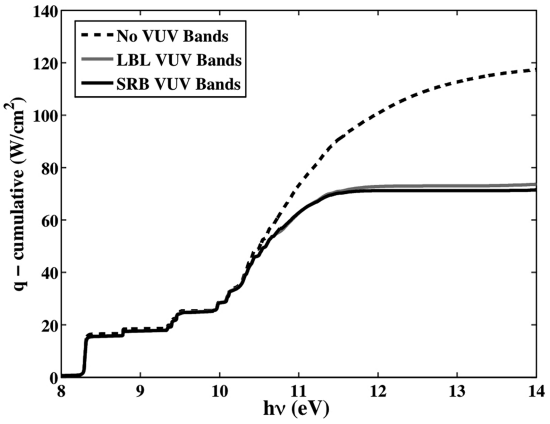

b) Cumulative flux

Fig. 6 Comparison of the VUV flux from layer 2 predicted by the LBL and SRB band models, with $\alpha = 0.4$ and $T_2 = 5000$ K.

T_2 values. This good agreement provides confidence in the application of the SRB model to an ablating boundary layer.

In summary, the analysis presented in this section has shown that an ablation-contaminated boundary layer absorbs significantly in the 6–18 eV range for a wide range of conditions. The radiation in the 0–6 eV range, however, was shown to provide net emission for most cases. Moreover, the magnitude of this emission was shown to be very sensitive to the temperature and abundance of ablation species. The counteracting influence of emission in the 0–6 eV range and absorption in the 6–18 eV range, and the inherent sensitivity of their net result, indicates how previous studies have predicted both increases [13,14] and decreases [12] in the radiative heating with the introduction of ablation species. It should also be noted that, although not presented, similar trends with α and T_2 were obtained using the equilibrium chemistry and radiation models of the RAD/EQUIL code [75]. Finally, the validity of the SRB model for treating absorbing VUV-band systems was shown.

V. Mars-Return Benchmark Case

To provide confidence in the coupled radiation and ablation flowfield model discussed in Secs. II and III, the developed model was applied to a widely studied Mars-return case. This case consists of the flow past a 3.05-m sphere with a freestream velocity of 15.24 km/s, a density of 2.55×10^{-4} kg/m^3 (altitude= 60.96 km), and a wall temperature of 3600 K. The injected gas is carbon-phenolic with elemental mass fractions specified as C/H/O/N = 0.92/0.022/0.049/0.009.

The combination of the high flight velocity, relatively high freestream density, and large body size results in a highly thermochemical equilibrium flowfield that is coupled strongly to the radiation. The strong thermochemical equilibrium conditions cause sharp gradients in the temperatures and number densities at the shock (as a result of the abrupt change from the freestream quantities to the postshock quantities), which were found to cause stability problems in the flowfield solution procedure. To accommodate this, the recently developed [32] general chemical equilibrium option in LAURA was applied. This option treats a single temperature and solves the elemental continuity equations. The same 22 species listed in Sec. II are applied. To maintain stability in the solution procedure, a 128-point grid normal to the body was implemented, instead of the commonly applied 64-point grid. Note that all previous studies of this case [6,9,76,77] avoided these stability issues by applying discrete-shock viscous-shock-layer flowfield models, which do not require the continuous treatment of the freestream to postshock transition.

The influences of both coupled ablation and radiation on the stagnation-line temperature and wall-directed radiative flux profiles are shown in Figs. 7 and 8. Significant decreases in the temperature and radiative flux profiles, as well as the shock standoff distance, are seen to result from the radiation coupling (all cases shown include radiation coupling except for the "No Rad." case). The introduction of ablation is shown to increase the shock standoff while absorbing roughly 40% of the radiative flux. The equilibrium viscous-shock-layer results of Moss [9] are also shown in these figures, where available. Considering the different flowfield, radiation, and thermophysical property models applied by Moss, the comparison with the present results is very good. A further comparison between the present results and those of Moss is shown in Fig. 9. The ablation mass fractions shown in this figure are defined as the sum of the following mass fractions: C, C^+, CO, CO_2, C_2, C_3, C_2H, CN, H, and H_2. For all three ablation rates, the agreement with Moss is good.

A comparison of the radiative flux at the wall predicted by various researchers is shown in Fig. 10 for various ablation rates. For the radiation calculation, Gupta et al. [10] and Sutton [76] applied the RAD/EQUIL code [75], Moss [9] applied the LRAD-3 code [77], and Garrett et al. [6] applied the RATRAP code [1]. The results of the various studies, including the present study, agree within about 10% for the entire range of ablation rates.

The excellent agreement shown in Figs. 7–10 with previous viscous-shock-layer results for this case, which includes extreme ablation and radiation coupling, provides a level of confidence in the present analysis. The present case considered a simple axisymmetric stagnation region flow, which minimizes the influence of the approximations inherent in the viscous-shock-layer analyses. As a result, it is not surprising that the present Navier–Stokes results agree well with the viscous-shock-layer results (assuming the radiation, transport, and thermodynamic properties applied are similar). The advantage of the present Navier–Stokes analysis is that it may be applied to complex geometries and thermochemical nonequilibrium cases, both of which these past viscous-shock-layer studies could not treat. To the knowledge of the authors, this is the first analysis of the present Mars-return case using a shock-capturing Navier–Stokes flowfield (although a similar case without ablation was treated in this way by Gollan et al. [78], and a lower velocity and density Mars-return case was treated by Hartung et al. [79], also without ablation).

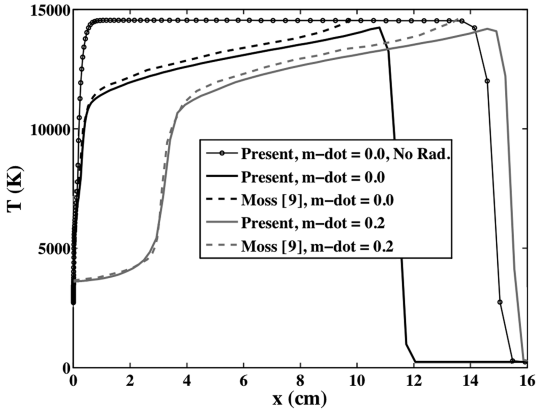

Fig. 7 Temperature distributions along the stagnation line with and without radiation and ablation.

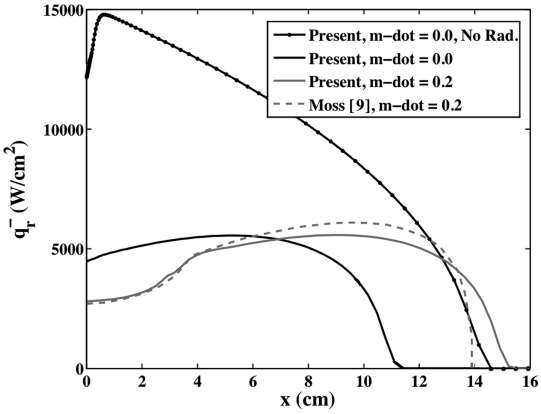

Fig. 8 Wall-directed radiative flux along the stagnation line with and without radiation and ablation.

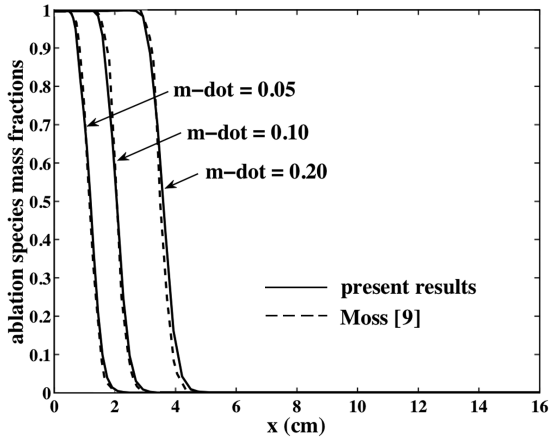

Fig. 9 Mass fraction of ablation species along the stagnation line.

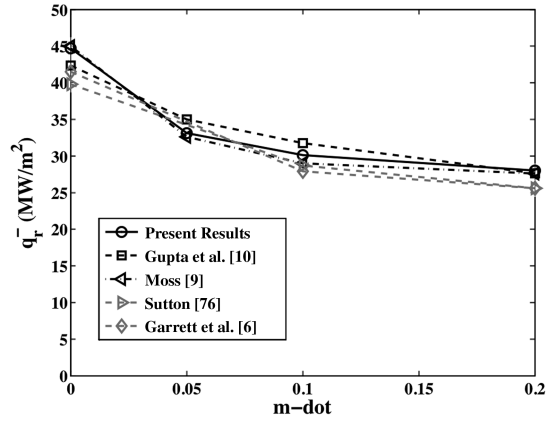

Fig. 10 Wall-directed radiative flux at the stagnation point.

VI. Apollo 4 Peak-Heating Analysis

The Apollo 4 flight experiment at $t = 30,032$ s is studied assuming the stagnation region flowfield is approximated with a 3-m sphere [80]. The two-temperature thermochemical nonequilibrium model in LAURA is applied. A freestream velocity of 10.252 km/s and a density of 3.41×10^{-4} kg/m^3 are applied. Following Park [11], a wall temperature of 2500 K is assumed, and the total ablation rate is assumed to be composed of 60% pyrolysis gas and 40% char. The elemental mass fractions are specified for the char as [81] C/H/O/N = 0.75/0.00/0.25/0.00 and for the pyrolysis gas as C/H/O/N = 0.547/0.093/0.341/0.019. The silicon present in the char, according to [81], is treated in the present analysis as carbon. The *m-dot* values considered were varied from the value of 0.0086 suggested by Park [11] to a value 4 times greater. Coupled radiation is included in the results presented here unless stated otherwise.

The number densities along the stagnation-line near the wall (only 3 cm of the 16-cm shock layer is shown), resulting from *m-dot* = 0.0086, are shown in Fig. 11 for the ablation species and Fig. 12 for the air species. It is seen that CO, H_2, and C_3 are the most abundant of the ablation species molecules at and very near the wall, which is significant because they each have strongly absorbing VUV-band systems. The impact of these band systems on the radiative heating will be shown later in this section.

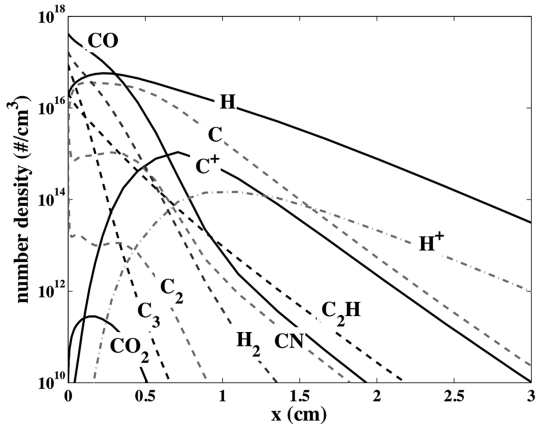

Fig. 11 Ablation species number densities along the stagnation line for the *m-dot* = 0.0086 case.

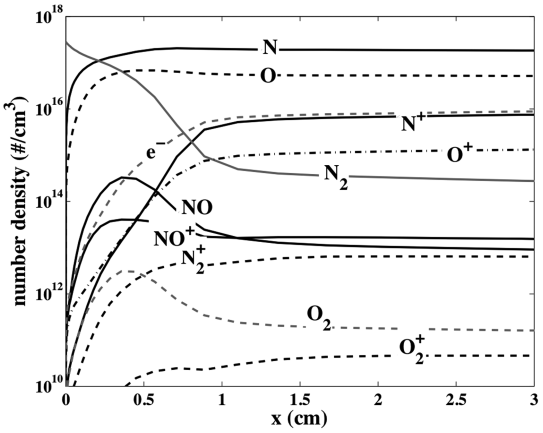

Fig. 12 Air species number densities along the stagnation line for the *m-dot* = 0.0086 case.

The elemental mass fractions near the wall are shown in Fig. 13 for *m-dot* values of 0.00, 0086, and 0.017. This shows that nitrogen is reduced to accommodate the injected carbon and hydrogen, while the oxygen content is actually slightly increased because it composes a significant fraction of the pyrolysis gas. Note that, even for the *m-dot* = 0.0 case, the elemental mass fractions of N and O are not constant through the boundary layer as a result of multicomponent diffusion. The resulting temperature profiles near the wall for these three *m-dot* cases are shown in Fig. 14. For the case with no ablation (*m-dot* = 0.0), the T_{tr} and T_{ve} profiles remain essentially identical

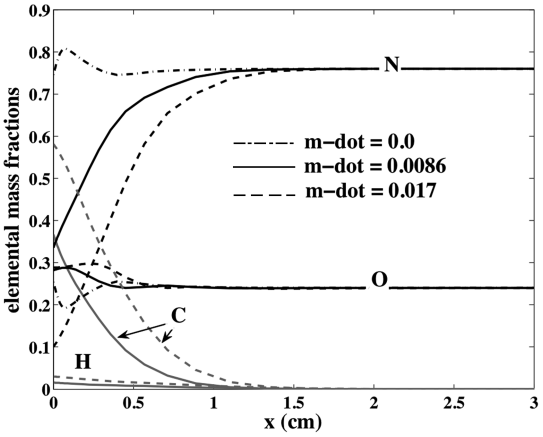

Fig. 13 Elemental mass fractions along the stagnation line for various ablation rates.

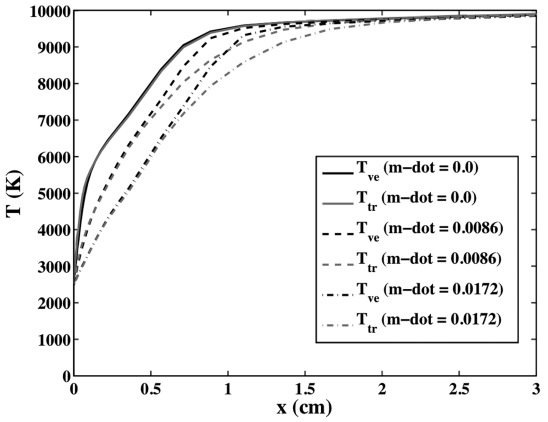

Fig. 14 Temperature profiles along the stagnation line for various ablation rates.

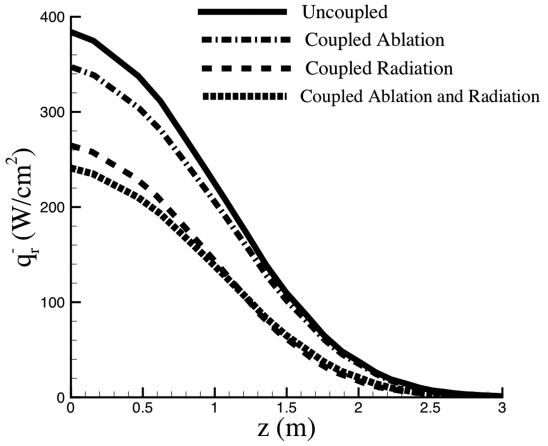

Fig. 15 Radiative flux along the body for cases with and without coupled radiation and ablation (with *m-dot* = 0.0086).

throughout the boundary layer, whereas, for the ablation cases, there is noticeable separation at the boundary-layer edge.

The impact of coupled ablation and radiation flowfields on the radiation and convective heating are shown in Figs. 15 and 16, respectively, for *m-dot* = 0.0086. Focusing of the stagnation region ($z < 0.5$ m), Fig. 15 shows that the introduction of coupled ablation reduces the radiative heating by 7–9% (depending on whether coupled radiation is considered), whereas coupled radiation reduces it by 30%. Together, the coupled radiation and ablation reduce the uncoupled radiation by 140 W/cm^2, or 37%, at the stagnation point ($z = 0$). For convective heating, Fig. 16 shows that coupled ablation provides a significant decrease, whereas the influence of coupled radiation is minimal. The small influence of coupled radiation on the convective heating predicted in this study, with and without coupled ablation, is in disagreement with the results of Park [11]. Together, the coupled radiation and ablation reduce the uncoupled convective heating by 90 W/cm^2, or 38%, at the stagnation point. Note that the uncoupled ablation cases apply an equilibrium catalytic wall boundary condition. Considering both the convective and radiative heating, coupled radiation and ablation provide a decrease from 620 to 390 W/cm^2, or 37%, at the stagnation point.

The influence of varying *m-dot* on the radiative heating is shown in Fig. 17. Even for the largest *m-dot* of 0.0344, the radiation is reduced by only 19% at the stagnation point (relative to the *m-dot* = 0.0 case). Details of this reduction are discussed in the next paragraph. For the convective heating, the influence of varying *m-dot* is shown in Fig. 18. As expected, increasing *m-dot* significantly decreases the convective heating. The three circles in this figure indicate the stagnation-point convective heating predicted with the thin-film blowing correction (with $\lambda = 0.5$) [44,82], which is applied to the *m-dot* = 0.0 case to approximate the influence of

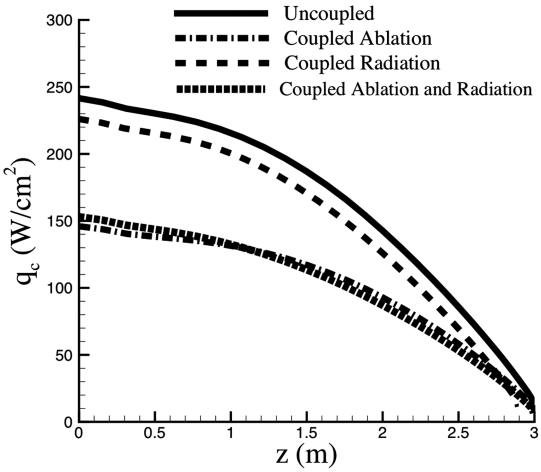

Fig. 16 Convective heating along the body for cases with and without coupled radiation and ablation (with *m-dot* = 0.0086).

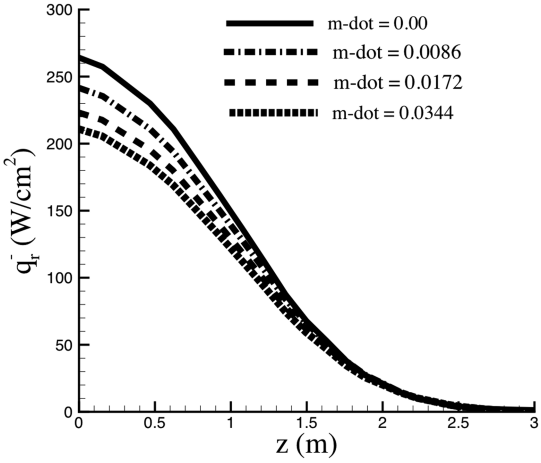

Fig. 17 Radiative flux along the body for various blowing rates with coupled radiation.

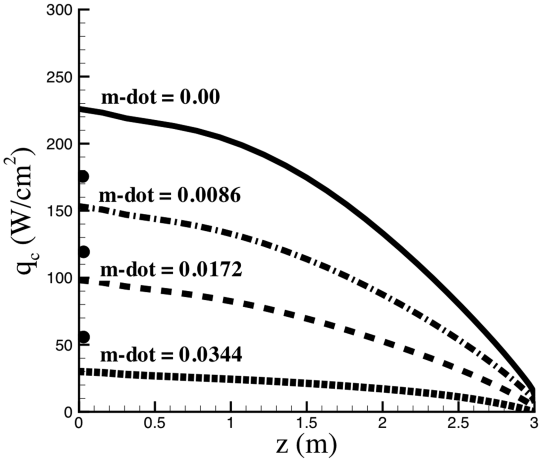

Fig. 18 Convective heating along the body for various blowing rates with coupled radiation.

ablation. Each of the circles corresponds to the *m-dot* value and actual coupled ablation prediction (represented by the lines) located directly below it. The blowing correction is seen to result in convective heating values 15–50% larger than the coupled ablation predictions. This discrepancy indicates that the blowing correction, as applied with $\lambda = 0.5$, is inadequate at the present conditions.

The influence of the ablation species on the radiative heating is studied further in Figs. 19 and 20, which show the influence of adding the radiation mechanisms from the identified species (only the dominant contributing species are shown). The flux obtained by ignoring the ablation species in the radiation calculation is represented by the dashed line, and the increment obtained by adding the radiation from the identified species is shown by the arrows. The dash-dotted line represents the flux obtained accounting for all of the ablation species. For the integrated flux from the 0–6 eV range shown in Fig. 19, the ablation species are seen to cause a relatively small increase (note the limits of the vertical scale) in the flux. The largest contributors to this increase are CN and C, whereas C_3 actually absorbs slightly. For the integrated flux between 6–18 eV, Fig. 20 shows the flux reduction indicated previously in Fig. 17. The photoionization of C causes a significant fraction of this absorption, while the vacuum-ultraviolet-band systems of CO, C_3, and H_2 also contribute noticeably.

To complete this analysis of the Apollo 4 radiative heating, a comparison is made with the radiometer flight data, which measured the radiative intensity between 0.4 and 6.2 eV at the stagnation point. As pointed out by Park [11], the radiometer window was located in an open cavity 8 cm from the wall. The assumption is made here that the gas in the open cavity was in equilibrium at the wall temperature (2500 K), pressure (0.34 atm), and elemental mass fractions (C:H:O:N = 0.37:0.01:0.28:0.34) for the *m-dot* = 0.0086 case. The resulting cumulative intensity, considering coupled ablation and radiation, is shown in Fig. 21. Excellent agreement is seen between the prediction at the radiometer and the radiometer measurement. The absorption in the radiometer cavity is indicated by the difference between the prediction at the wall and at the radiometer window. The absorption in the radiometer cavity is due almost entirely to the C_3 Swings band system.

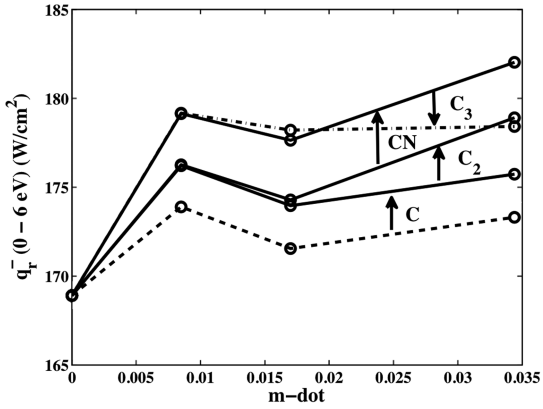

Fig. 19 Influence of including the radiation mechanisms of various species on the stagnation-point radiative flux between 0 and 6 eV.

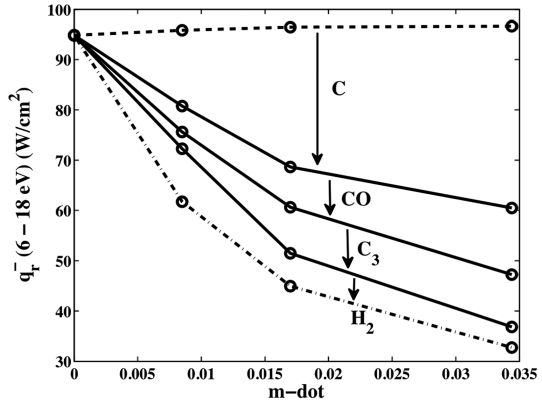

Fig. 20 Influence of including the radiation mechanisms of various species on the stagnation-point radiative flux between 6 and 18 eV.

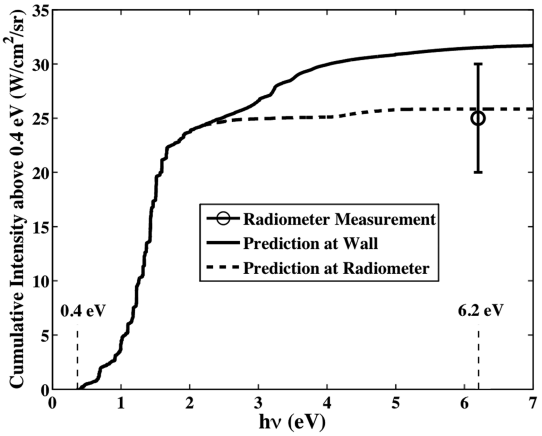

Fig. 21 Cumulative intensity above 0.4 eV for the Apollo 4 case with coupled ablation (*m-dot* = 0.0086) and radiation.

If carbonaceous species were not present in the radiometer cavity, as Park [11] suggests, then the absorption would be negligible and the present results would then overpredict the data by about 7 $W/cm^2/sr$. This agreement is still relatively good and agrees closely with the results of Park [11]. As mentioned in Sec. III, the present predictions apply an atomic line model that includes additional lines from the Opacity Project that are not present in the NIST database. These lines contribute 2.5 W/cm^2 to the present case between 0.4 and 6.2 eV. Also, the negative nitrogen ion photodetachment contribution is included, which contributes 1.4 $W/cm^2/sr$ for present case. The accuracy of the modeling data for these additional lines, as well as the negative ion cross section, is questionable and these contributions are often ignored completely, although they are included in HARA for conservatism. If these contributions are ignored along with the radiometer cavity absorption, good agreement with the flight data is obtained. However, previous comparisons with the Fire II flight data [83] support the inclusion of these contributions.

VII. Conclusions

The influence of ablation on the radiative heating for lunar- and Mars-return conditions was studied using state-of-the-art flowfield (LAURA) and radiation (HARA) models. In addition, a simplified shock-layer model was studied to clearly indicate the radiation characteristics of an ablation-contaminated boundary layer. This simplified model showed that, with ablation, the boundary layer in the 0–6 eV range was capable of providing a net emission for a wide range of temperatures. The 6–18 eV range, however, was shown to provide significant absorption for all cases, which actually became stronger with the increase of ablation species. These counteracting influences (the increased flux between 0–6 eV and the decreased flux between 6–18 eV), and the sensitivity of their net result to temperature and gas composition, explain how previous studies predicted both increases and decreases in the radiation with the introduction of ablation. Also shown using this simplified model was that the SRB treatment of molecular band systems in the VUV results in spectrally integrated radiative flux values within 3% of the computationally expensive LBL model.

A 22-species LAURA flowfield model, with coupled ablation and radiation, was applied to a Mars-return case, which was widely studied in the 1970s using viscous-shock-layer techniques. Excellent agreement with the results of Moss [9] was found for stagnation-line temperature, ablation species, and radiative flux profiles. Furthermore, good agreement with numerous previous viscous-shock-layer studies was shown for the wall radiative flux values predicted with various ablation rates. The influence of coupled radiation and ablation for these cases was large; thus, this good agreement provided confidence in the recently developed coupled ablation and radiation procedure in LAURA.

The influence of coupled ablation and radiation on the radiative and convective heating for the Apollo 4 peak-heating case was examined. Increasing the ablation rate *m-dot* from 0.0 to 0.0344 was shown to decrease the radiative heating by 15%, while decreasing the convective heating by 85%. The introduction of coupled radiation was found to decrease the radiative heating by 30%, while having a negligible influence on the convective heating. Excellent agreement between the present predictions and the Apollo 4 radiometer data was shown. This good agreement included absorption from the open radiometer cavity, which was assumed to contain gas at the temperature, pressure, and elemental composition of the wall.

References

[1] Hoshizaki, H., and Lasher, L. E., "Convective and Radiative Heat Transfer to an Ablating Body," *AIAA Journal*, Vol. 6, No. 8, 1968, pp. 1441–1449. doi:10.2514/3.4786

[2] Wilson, K. H., and Hoshizaki, H., "Effect of Ablation Product Absorption and Line Transitions on Shock Layer Radiative Transport," NASA CR-1264, 1969.

[3] Chin, J. H., "Radiation Transport for Stagnation Flows Including Effects of Lines and Ablation Layer," *AIAA Journal*, Vol. 7, No. 7, 1969, pp. 1310–1318. doi:10.2514/3.5339

[4] Rigdon, W. S., Dirling, R. B., and Thomas, M., "Stagnation Point Heat Transfer During Hypervelocity Atmospheric Entry," NASA CR-1462, 1970.

[5] Smith, G. L., Suttles, J. T., Sullivan, E. M., and Graves, R. A., "Viscous Radiating Flowfield on an Ablating Blunt Body," AIAA Paper 70-218, 1970.

[6] Garrett, L. B., Smith, G. L., and Perkins, J. N., "An Implicit Finite-Difference Solution to the Viscous Shock Layer, Including the Effects of Radiation and Strong Blowing," NASA TR R-388, 1972.

[7] Engel, C. D., Farmer, C. F., and Pike, R. W., "Ablation and Radiation Coupled Viscous Hypersonic Shock Layers," *AIAA Journal*, Vol. 11, No. 8, 1973, pp. 1174–1181. doi:10.2514/3.6889

[8] Moss, J. N., "The Effect of Ablation Injection on Radiative and Convective Heating," NASA TM X-71976, June 1974.

[9] Moss, J. N., "Radiative Viscous-Shock-Layer Solutions with Coupled Mass Ablation," *AIAA Journal*, Vol. 14, No. 9, 1976, pp. 1311–1317. doi:10.2514/3.61464

[10] Gupta, R. N., Lee, K. P., Moss, J. N., and Sutton, K., "Viscous Shock Layer Solutions with Coupled Radiation and Ablation Injection for Earth Entry," *Journal of Spacecraft and Rockets*, Vol. 29, No. 2, 1992, pp. 173–181. doi:10.2514/3.26332

[11] Park, C., "Stagnation-Point Radiation for Apollo 4," *Journal of Thermophysics and Heat Transfer*, Vol. 18, No. 3, 2004, pp. 349–357. doi:10.2514/1.6527

[12] Park, C., "Calculation of Stagnation-Point Heating Rates Associated with Stardust Vehicle," *Journal of Spacecraft and Rockets*, Vol. 44, No. 1, 2007, pp. 24–32. doi:10.2514/1.15745

[13] Olynick, D., Chen, Y.-K., and Tauber, M. E., "Aerothermodynamics of the Stardust Sample Return Capsule," *Journal of Spacecraft and Rockets*, Vol. 36, No. 3, 1999, pp. 442–462. doi:10.2514/2.3466

[14] Gupta, R. N., "Aerothermodynamic Analysis of Stardust Sample Return Capsule with Coupled Radiation and Ablation," *Journal of Spacecraft and Rockets*, Vol. 37, No. 4, 2000, pp. 507–514. doi:10.2514/2.3592

[15] Doihara, R., and Nishida, M., "Ablation Studies for a Super-Orbital Reentry Capsule Using a Three-Temperature Model," *Transactions of the Japan Society for Aeronautical and Space Sciences*, Vol. 47, No. 157, 2004, pp. 161–166. doi:10.2322/tjsass.47.161

[16] Park, C., Abe, T., and Inatani, Y., "Research on the Heatshield for MUSES-C Earth Reentry," AIAA Paper 98-2852, 1998.

[17] Otsu, H., Suzuki, K., Fujita, K., and Abe, T., "Effect of Ablative Gas on the Radiative Environment Around the MUSES-C Reentry Capsule," AIAA Paper 1999-3463, 1999.

[18] Fujita, K., Abe, T., and Suzuki, K., "Air Radiation Analysis of a Superorbital Reentry Vehicle," AIAA Paper 97-2561, 1997.

[19] Nicolet, W. E., "Aerothermodynamic Environment for Jovian Entry Conditions," AIAA Paper 75-672, 1975.

[20] Moss, J. N., Anderson, E. C., and Bolz, C. W., "Aerothermal Environment for Jovian Entry Probes," AIAA Paper 76-469, 1976.
[21] Moss, J. N., Jones, J. J., and Simmonds, A. L., "Radiative Flux Penetrations Through a Blown Shock Layer for Jupiter Entry Conditions," AIAA Paper 78-908, 1978.
[22] Arnold, J. O., Cooper, D. M., Park, C., and Prakash, S. G., "Line-by-Line Transport Calculations for Jupiter Entry Probes," AIAA Paper 79-1082, 1979.
[23] Moss, J. N., Simmonds, A. L., and Anderson, E. C., "Turbulent Radiating Shock Layers with Coupled Ablation Injection," *Journal of Spacecraft and Rockets*, Vol. 17, No. 3, 1980, pp. 177–183. doi:10.2514/3.57726
[24] Matsuyama, S., Ohnishi, N., Sasoh, A., and Sawada, K., "Numerical Simulation of Galileo Probe Entry Flowfield with Radiation and Ablation," *Journal of Thermophysics and Heat Transfer*, Vol. 19, No. 1, 2005, pp. 28–35. doi:10.2514/1.10264
[25] Moss, J. N., Zoby, E. V., Sutton, K., and Anderson, E. C., "Aerothermal Environments for the Pioneer-Venus Multiprobe Mission," AIAA Paper 77-766, 1977.
[26] Park, C., and Ahn, H.-K., "Stagnation-Point Heat Transfer Rates for Pioneer-Venus Probes," *Journal of Thermophysics and Heat Transfer*, Vol. 13, No. 1, 1999, pp. 33–41. doi:10.2514/2.6426
[27] Sutton, K., "Coupled Nongray Radiating Flows About Ablating Planetary Entry Bodies," *AIAA Journal*, Vol. 12, No. 8, 1974, pp. 1099–1105. doi:10.2514/3.49419
[28] Fujita, K., Sumi, T., Yamada, T., and Ishii, N., "Assessment of Heating Environments of a Venus Entry Capsule for a Trail Balloon Mission," AIAA Paper 2005-5207, 2005.
[29] Fujita, K., Yamada, T., and Ishii, N., "Impacts of Ablation Gas Kinetics on Hyperbolic Entry Radiative Heating," AIAA Paper 2006-1185, 2006.
[30] Fujita, K., Matsukawa, Y., Yamada, T., and Ishii, N., "Evaluation of Heat Transfer Rates of Venus Entry Capsules Along Flight Trajectories," AIAA Paper 2006-3580, 2006.
[31] Gupta, R. N., Lee, K. P., Moss, J. N., and Sutton, K., "Viscous Shock Layer Analysis of the Martian Aerothermal Environment," *Journal of Spacecraft and Rockets*, Vol. 29, No. 5, 1992, pp. 633–640. doi:10.2514/3.11503
[32] Gnoffo, P. A., Johnston, C. O., and Thompson, R. A., "Implementation of Radiation, Ablation, and Free Energy Minimization Modules for Coupled Simulations of Hypersonic Flow," AIAA Paper 2009-1399, Jan. 2009.
[33] Cheatwood, F. M., and Gnoffo, P. A., "User's Manual for the Langley Aerothermodynamic Upwind Relaxation Algorithm (LAURA)," NASA TM 4674, April 1996.
[34] Gnoffo, P. A., Gupta, R. N., and Shinn, J. L., "Conservation Equations and Physical Models for Hypersonic Air Flows in Thermal and Chemical Nonequilibrium," NASA TP 2867, Feb. 1989.
[35] Roe, P. L., "Approximate Riemann Solvers, Parameter Vectors, and Difference Schemes," *Journal of Computational Physics*, Vol. 43, No. 2, Oct. 1981, pp. 357–372. doi:10.1016/0021-9991(81)90128-5
[36] Yee, H. C., "On Symmetric and Upwind TVD Schemes," NASA TM 88325, 1986.
[37] Park, C., "Review of Chemical-Kinetic Problems of Future NASA Missions, I: Earth Entries," *Journal of Thermophysics and Heat Transfer*, Vol. 7, No. 3, 1993, pp. 385–398. doi:10.2514/3.431
[38] Park, C., Jaffe, R. L., and Partridge, H., "Chemical-Kinetic Parameters of Hyperbolic Earth Entry," *Journal of Thermophysics and Heat Transfer*, Vol. 15, No. 1, 2001, pp. 76–90. doi:10.2514/2.6582
[39] Park, C., Howe, J. T., Jaffe, R. L., and Candler, G. V., "Review of Chemical-Kinetic Problems of Future NASA Missions, II: Mars Entries," *Journal of Thermophysics and Heat Transfer*, Vol. 8, No. 1, 1994, pp. 9–23. doi:10.2514/3.496
[40] Gokcen, T., "N2-CH4-Ar Chemical Kinetic Model for Simulations of Titan Atmospheric Entry," *Journal of Thermophysics and Heat Transfer*, Vol. 21, No. 1, 2007, pp. 9–18. doi:10.2514/1.22095
[41] Mcbride, B. J., Zehe, M. J., and Gordon, S., "NASA Glenn Coefficients for Calculating Thermodynamic Properties of Individual Species," NASA TP 2002-211556, Sept. 2002.
[42] Gupta, R. N., Yos, J. M., Thompson, R. A., and Lee, K. P., "A Review of Reaction Rates and Thermodynamic and Transport Properties for an 11-Species Air Model for Chemical and Thermal Nonequilibrium Calculations to 30,000 K," NASA RP-1232, 1990.
[43] Sutton, K., and Gnoffo, P. A., "Multi-Component Diffusion with Application to Computational Aerothermodynamics," AIAA Paper 98-2575, 1998.
[44] Thompson, R. A., and Gnoffo, P. A., "Implementation of Blowing Boundary Condition in the LAURA Code," AIAA Paper 2008-1243, 2008.
[45] Moss, J. N., "Reacting Viscous-Shock-Layer Solutions with Multicomponent Diffusion and Mass Injection," NASA TR R-411, 1974.
[46] Johnston, C. O., Hollis, B. R., and Sutton, K., "Spectrum Modeling for Air Shock Layers at Lunar Return Conditions," *Journal of Spacecraft and Rockets*, Vol. 45, No. 5, 2008, pp. 865–878. doi:10.2514/1.33004
[47] Johnston, C. O., Hollis, B. R., and Sutton, K., "Non-Boltzmann Modeling for Air Shock Layers at Lunar Return Conditions," *Journal of Spacecraft and Rockets*, Vol. 45, No. 5, 2008, pp. 879–890. doi:10.2514/1.33006
[48] NIST Atomic Spectra Database [online database], http://physics.nist.gov/PhysRefData/ASD/index.html, July 2006 [retrieved 3 Sept. 2006].
[49] Opacity Project Team, *The Opacity Project*, Vol. 1, Inst. of Physics Publishing, London, 1995.
[50] Cunto, W., Mendoza, C., Ochsenbein, F., and Zeippen, C. J., "TOPbase at the CDS," *Astronomy and Astrophysics*, Vol. 275, 1993, pp. L5–L8.
[51] Soon, W. H., and Kunc, J. A., "Nitrogen Plasma Continuum Emission Associated with N-(3P) and N-(1D) Ions," *Physical Review A*, Vol. 41, No. 8, 1990, pp. 4531–4533. doi:10.1103/PhysRevA.41.4531
[52] Chauveau, S., Deron, C., Perrin, M.-Y., Riviere, P., and Soufiani, A., "Radiative Transfer in LTE Air Plasmas for Temperatures up to 15,000 K," *Journal of Quantitative Spectroscopy and Radiative Transfer*, Vol. 77, No. 2, 2003, pp. 113–130. doi:10.1016/S0022-4073(02)00080-8
[53] Chambers, L. H., "Predicting Radiative Heat Transfer in Thermochemical Nonequilibrium Flow Fields," NASA TM-4564, 1994.
[54] Laux, C. O., "Optical Diagnostics and Radiative Emission of Air Plasmas," High Temperature Gas Dynamics Lab, Mechanical Engineering Dept., Stanford University, Rept. T-288, 1993.
[55] Whang, T. J., Guoxing, Z., Stwalley, W. C., and Wu, C. Y. R., "Franck-Condon Factors of the $b\prime 1\Sigma u + -X1\Sigma g+$, $c31\Pi u - X1\Sigma g+$, $c\prime 41\Sigma u + -X1\Sigma g+$, $c\prime 41\Sigma u + -a1\Pi g$, and $o31\Pi u - X1\Sigma g+$ Transitions of N_2," *Journal of Quantitative Spectroscopy and Radiative Transfer*, Vol. 55, No. 3, 1996, pp. 335–344. doi:10.1016/0022-4073(95)00169-7
[56] Stahel, D., Leoni, M., and Dresslar, K., "Nonadiabatic Representations of the $^1\Sigma_u$ and $^1\Pi_u$ States of the N_2 Molecule," *Journal of Chemical Physics*, Vol. 79, No. 6, Sept. 1983, pp. 2541–2558. doi:10.1063/1.446166
[57] Chauveau, S., Perrin, M. Y., Riviere, P., and Soufiani, A., "Contributions of Diatomic Molecular Electronic Systems to Heated Air Radiation," *Journal of Quantitative Spectroscopy and Radiative Transfer*, Vol. 72, No. 4, 2002, pp. 503–530. doi:10.1016/S0022-4073(01)00141-8
[58] Park, C., "Radiation Enhancement by Nonequilibrium in Earth's Atmosphere," *Journal of Spacecraft and Rockets*, Vol. 22, No. 1, 1985, pp. 27–36. doi:10.2514/3.25706
[59] Griem, H. R., *Spectral Line Broadening by Plasmas*, Academic Press, New York, 1974.
[60] Wilson, K. H., and Nicolet, W. E., "Spectral Absorption Coefficients of Carbon, Nitrogen, and Oxygen Atoms," *Journal of Quantitative Spectroscopy and Radiative Transfer*, Vol. 7, No. 6, 1967, pp. 891–941. doi:10.1016/0022-4073(67)90005-2
[61] Sutton, K., "Approximate Line Shapes for Hydrogen," *Journal of Quantitative Spectroscopy and Radiative Transfer*, Vol. 20, No. 4, 1978, pp. 333–343. doi:10.1016/0022-4073(78)90102-4
[62] Lino da Silvia, M., and Dudeck, M., "Arrays of Radiative Transition Probabilities for $CO_2 - N_2$ Plasmas," *Journal of Quantitative Spectroscopy and Radiative Transfer*, Vol. 102, No. 3, 2006, pp. 348–386. doi:10.1016/j.jqsrt.2006.02.018
[63] Park, C., "Radiation Intensity Parameter Tables for Carbon Monoxide," *Proceedings of the International Workshop on Radiation of High Temperature Gases in Atmospheric Entry*, Pt. 2, Oct. 2005.
[64] Cooper, D. M., and Jones, J. J., "An Experimental Determination of the Cross Section of the Swings Band System of C_3," *Journal of*

Quantitative Spectroscopy and Radiative Transfer, Vol. 22, No. 2, 1979, pp. 201–208.
doi:10.1016/0022-4073(79)90042-6

[65] Shinn, J. L., "Optical Absorption of Carbon and Hydrocarbon Species from Shock Heated Acetylene and Methane in the 135–220 nm Wavelength Range," AIAA Paper 81-1189, 1981.

[66] Prakash, S. G., and Park, C., "Shock Tube Spectroscopy of $C_3 + C_2H$ Mixture in the 140–700 nm Range," AIAA Paper 79-0094, 1979.

[67] Allison, A. C., and Dalgarno, A., "Band Oscillator Strengths and Transitions Probabilities for the Lyman and Werner Systems of H_2, HD, and D_2," *Atomic Data*, Vol. 1, No. 3, 1970, pp. 289–304.

[68] Park, C., "Interaction of Spalled Particles with Shock Layer Flow," *Journal of Thermophysics and Heat Transfer*, Vol. 13, No. 4, 1999, pp. 441–448.
doi:10.2514/2.6482

[69] Park, C., Raiche, G. A., and Driver, D. M., "Radiation of Spalled Particles in Shock Layers," *Journal of Thermophysics and Heat Transfer*, Vol. 18, No. 4, 2004, pp. 519–526.
doi:10.2514/1.8098

[70] Kontinos, D. A., and Stackpole, M., "Post-Flight Analysis of the Stardust Sample Return Capsule Earth Entry," AIAA Paper 2008-1197, 2008.

[71] Liu, Y., Prabhu, D., Trumble, K. A., Saunders, D., and Jenniskens, P., "Radiation Modeling for the Reentry of the Stardust Sample Return Capsule," AIAA Paper 2008-1213, 2008.

[72] Nelson, H. F., "Radiation Transfer Through Carbon Ablation Layers," *Journal of Quantitative Spectroscopy and Radiative Transfer*, Vol. 13, No. 5, 1973, pp. 427–445.
doi:10.1016/0022-4073(73)90005-8

[73] Funatsu, M., and Hiroyuki, S., "Radiative and Absorptive Characteristics of Ablation Layers of SiC Heat Sheild," AIAA Paper 2001-1776, 2001.

[74] Johnston, C. O., Hollis, B. R., and Sutton, K., "Radiative Heating Methodology for the Huygens Probe," *Journal of Spacecraft and Rockets*, Vol. 44, No. 5, 2007, pp. 993–1002.
doi:10.2514/1.26424

[75] Nicolet, W. E., "Advanced Methods for Calculating Radiation Transport in Ablation-Product Contaminated Boundary Layers," NASA CR-1656, 1970.

[76] Sutton, K., "Characteristics of Coupled Nongray Radiating Gas Flows with Ablation Product Effects About Blunt Bodies," Ph.D. Dissertation, North Carolina State Univ., Raleigh, NC, 1973.

[77] Engel, C. D., Farmer, R. C., and Pike, R. W., "Ablation and Radiation Coupled Viscous Hypersonic Shock Layers," NASA CR-112306, 1971.

[78] Gollan, R. J., Jacobs, P. A., Karl, S., and Smith, S. C., "Numerical Modelling of Radiating Superorbital Flows," *ANZIAM Journal*, Vol. 45, E, 2004, pp. C248–C268.

[79] Hartung, L. C., Mitcheltree, R. A., and Gnoffo, P. A., "Coupled Radiation Effects in Thermochemical Nonequilibrium Shock-Capturing Flowfield Calculations," *Journal of Thermophysics and Heat Transfer*, Vol. 8, No. 2, 1994, pp. 244–250.
doi:10.2514/3.530

[80] Reid, R. C., Jr., Rochelle, W. C., and Milhoan, J. D., "Radiative Heating to the Apollo Command Module: Engineering Predictions and Flight Measurements," NASA TM X-58091, April 1972.

[81] Bartlett, E. P., Abbett, M. J., Nicolet, W. E., and Moyer, C. B., "Improved Heat Shield Design Procedures for Manned Entry Systems," NASA CR-108689, 1970.

[82] Milos, F. S., and Chen, Y.-K., "Two-Dimensional Ablation, Thermal Response, and Sizing Programs for Pyrolyzing Ablators," AIAA Paper 2008-1223, 2008.

[83] Johnston, C. O., Hollis, B. R., and Sutton, K., "Nonequilibrium Stagnation-Line Radiative Heating for Fire II," *Journal of Spacecraft and Rockets*, Vol. 45, No. 6, 2008, pp. 1185–1195.
doi:10.2514/1.33008

G. Palmer
Associate Editor